

ADVANCED LASER-DRIVEN PLASMA ACCELERATOR ELECTRON-BEAM DIAGNOSTICS WITH COTR-BASED TECHNIQUES*

A. H. Lumpkin[†], Fermi National Accelerator Laboratory, Batavia, IL, USA
M. LaBerge, M. Downer, University of Texas at Austin, Austin, TX, USA
D. W. Rule, Silver Spring, MD, USA
A. Irman, Helmholtz-Zentrum Dresden-Rossendorf, Dresden, Germany

Abstract

A significant advance in laser-driven plasma accelerator (LPA) electron-beam diagnostics has recently been demonstrated based on coherent optical transition radiation (COTR) imaging. We find COTR signal strengths from a microbunched subset of beam exiting the LPA to be several orders of magnitude higher than that of incoherent optical transition radiation (OTR). The transverse sizes are only a few microns as deduced from the point-spread-function-related lobe structure. In addition, the far-field COTR interferometric images obtained on the same shot provide beam-size limits plus divergence and pointing information at the sub-mrad level when compared to a modified analytical model. The integrated image intensities can be used to estimate the microbunching fraction and relatable to the LPA process. Initial results in a collaborative LPA experiment will be reported for electron beam energies of about 215 MeV. A revised configuration is proposed to record energy and energy spread via COTR on the same shot with the interferometer.

INTRODUCTION

The periodic longitudinal density modulation of relativistic electrons at the resonant wavelength (microbunching) is a well-known, fundamental aspect of free-electron lasers (FELs) [1]. In one classic case, microbunching fractions reached 20% at saturation of a self-amplified spontaneous emission (SASE) FEL resulting in gains of 10^6 at 530 nm [2]. In that experiment the concomitant z-dependent gain of coherent optical transition radiation (COTR) was also measured at the $>10^5$ level. Microbunching at visible wavelengths in laser-driven plasma accelerators (LPAs) had been reported previously [3,4], but it has only recently been measured in near-field and far-field images on a single shot for the first time with significant COTR enhancements involved [5-7].

We reintroduce a modified analytical model for COTR interferometry (COTRI) first developed for the SASE-FEL-induced microbunching case [8] to evaluate now the LPA case [7]. The coherence function was treated in this analytical model that addresses both cases and the expected fringe patterns. In the modified model, we consider the increase in the effective beam size in the drift between the foils due to the divergence term [9]. This term has negligible effects for low divergences of the

microbunched electrons.

In the FEL, one identified microbunched transverse cores of 25-100 microns in extent while in the LPA the recently reported transverse sizes at the exit of the LPA were a few microns [5-8]. In the latter case, signal enhancements $>10^5$ and extensive fringes out to 30 mrad in angle space were recorded.

EXPERIMENTAL ASPECTS

The LPA at HZDR

The LPA is based on the DRACO laser with a peak power of 150 TW at a central wavelength 800 nm interacting with a He gas jet (with 3% Nitrogen) at the Helmholtz-Zentrum Dresden-Rossendorf (HZDR) facility [10]. The LPA was operated with a plasma electron density $n_e \sim 3 \times 10^{18} \text{ cm}^{-3}$ in the self-truncated ionization-injection mode. Beam energies of ~ 215 MeV in a quasi-monoenergetic peak were observed in a downstream spectrometer. After the LPA, a 75- μm thin Al foil blocked the laser pulse and was followed by an Al-coated Kapton foil as shown in Fig. 1. The latter's back surface provided the source point of the near field (NF) COTR imaging, and a polished 200- μm thick Si mirror at 45° to the beam direction redirected this light to the microscope objective. The configuration provided a magnification factor of 42 at the camera and a calibration factor of 0.09 $\mu\text{m}/\text{pixel}$. This mirror was located 18.5 mm downstream of the Al-coated Kapton and also generated backward COTR that combined with the first source to provide COTRI in the far-field (FF) imaging camera. The significantly enhanced signal allowed the splitting of the signal into two NF cameras as well as a FF camera with a 633 ± 5 nm bandpass filter (BPF) as shown schematically in Fig. 2.

We propose an extension of the single-shot diagnostics coverage to electron beam energy, energy spread, and optical spectroscopy on the same shot by replacing the thick Si mirror at 45 degrees with a few- μm thin Al/Ti mirror/foil. This is so thin that the energy loss in transit for 215 MeV would be in the 10-4 range so energy spread info is also preserved. Since the scattering is much less than $1/\gamma$ we expect the microbunching fraction to be preserved also. An Al foil at the spectrometer focal plane and narrowband filter in front of the camera would allow the imaging of the COTR for the microbunched electrons.

* This manuscript has been authored by Fermi Research Alliance, LLC under Contract No. DE-AC02-07CH11359 with the U.S. Department of Energy, Office of Science, Office of High Energy Physics.

[†] lumpkin@fnal.gov

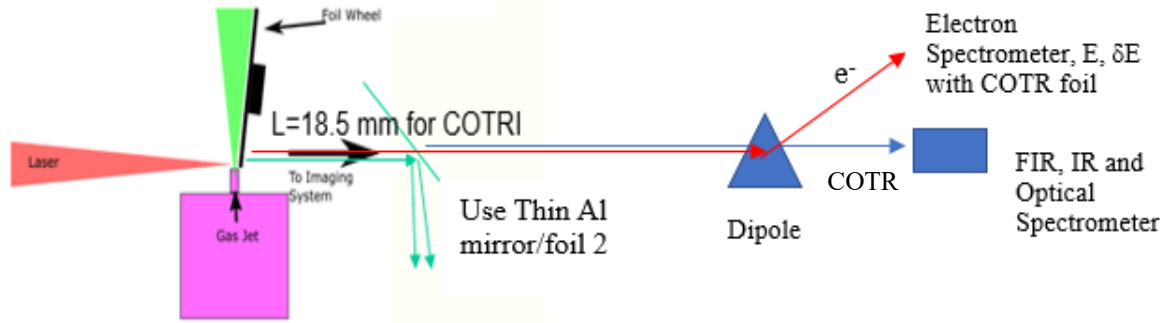


Figure 1: Schematic of an LPA showing the laser, gas jet, and foil geometry with a foil separation $L= 18.5$ mm for CO TRI [5,6]. The proposed *thin* second foil of the interferometer would enable the preservation of energy and microbunching aspects in the electrons for the downstream measurements on the same shot as the interferometer and generate the forward CO TR for the optical spectroscopy measurements.

Possible energy dispersion effects on the microbunching fraction need to be assessed. The electron beam continues to the Lanex screen for potential ensemble electron energy measurements and charge measurements.

where \hbar is Planck's constant/ 2π , e is electron charge, c is the speed of light, and θ_x and θ_y are radiation angles [11].

When N_b of the N particles are microbunched, a coherence function $\mathbf{J}(\mathbf{k})$ becomes involved, and for two foils an interference function $\mathbf{I}(\mathbf{k})$. The spectral angular distribution function then becomes

$$\frac{d^2W}{d\omega d\Omega} = |r_{\parallel,\perp}|^2 \frac{d^2W_1}{d\omega d\Omega} [N\mathbf{I}(\mathbf{k}) + N_b(N_b - 1)\mathbf{J}(\mathbf{k})] \quad (2)$$

where $|r_{\parallel,\perp}|^2$ is reflectance of the second (Si) foil for parallel, perpendicular polarization components, respectively. The reflectance reduces intensity of OTR from the first foil (via reflection from Si) and OTR generated at the Si wafer (via Eq. 2) equivalently. In the modified experimental configuration, this would be an Al foil, however with higher reflectance. $\mathbf{I}(\mathbf{k})$ is [11]

$$\mathbf{I}(\mathbf{k}) = 4 \sin^2 \left[\frac{kL}{4} (\gamma^{-2} + \theta_x^2 + \theta_y^2) \right] \quad (3)$$

where $k = |\mathbf{k}| = 2\pi/\lambda$, using a small-angle approximation. Choosing $L = 18.5$ mm provided good fringe contrast, while enabling near-field optics to focus on the first foil. The coherence function can be defined as

$$\mathbf{J}(\mathbf{k}) = (H_1(\mathbf{k}) - H_2(\mathbf{k}))^2 + H_1(\mathbf{k})H_2(\mathbf{k})\mathbf{I}(\mathbf{k}) \quad (4)$$

where $H_j(\mathbf{k}) = \rho_j(\mathbf{k})/Q = g_j(k_x)g_j(k_y)F(k_z)$ for a microbunch of charge distribution $\rho_j(x)$ and total charge Q , with $j = 1, 2$. Here we have introduced two microbunch form factors, H_1 and H_2 , to account for the increase in bunch radius from the first to the second interferometer foil due to beam divergence. Details of the Fourier transforms are in reference [7]. If $\mathbf{J}(\mathbf{k}) \ll 1$ or in Eq. (2). $N_b \rightarrow 0$, only the incoherent OTR term ($\sim N$) remains.

ANALYTICAL MODEL RESULTS

215-MeV CO TRI Results

Relevant former model results are shown in Fig. 3 illustrating the divergence effect on fringe visibility (negative angles) and the beam size effect on the enhancement of

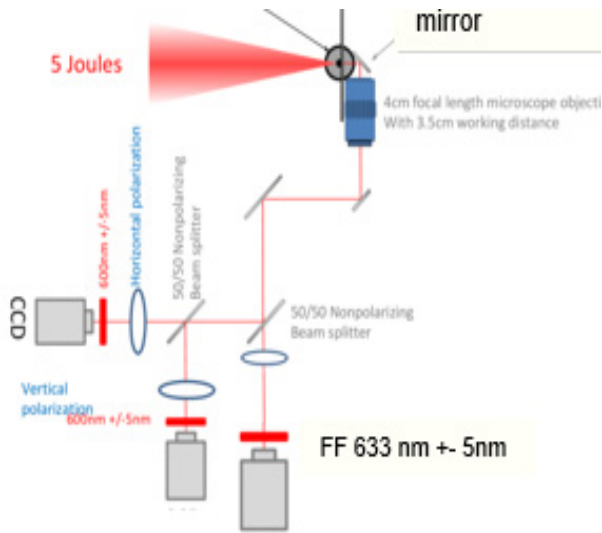


Figure 2: Schematic of the LPA and an early version of the NF and FF imaging setup using the beam splitters to redirect the optical signals to the different cameras [5,6]. The NF imaging could be used on the spectrometer screen.

MODIFIED ANALYTICAL MODEL

Currents induced when a charged particle beam enters and exits a foil generate backward and forward OTR in cones of half-angle $1/\gamma$ around the specular reflection and beam direction, respectively [11]. Thus, the configuration in Fig. 1 generates OTR at 90° to the beam direction, enabling minimally invasive OTR characterization. Upon exiting a foil, a single electron generates W_1 photons per unit frequency ω per unit solid angle Ω , as given by

$$\frac{d^2W_1}{d\omega d\Omega} = \frac{e^2}{\hbar c} \frac{1}{\pi^2 \omega} \frac{(\theta_x^2 + \theta_y^2)}{(\gamma^{-2} + \theta_x^2 + \theta_y^2)^2} \quad (1)$$

fringes (positive angles) at 215 MeV. One can see the fringe visibility is reduced for the 1.0-mrad case vs the 0.5-mrad case at the left. On the right, the coherence function is shown to be dramatically reduced at larger angles for the larger beam sizes. This means the FEL case only had a few visible fringes while the LPA fringe data extend out to 30 mrad. The foil separation was 18.5 mm and $\lambda = 633 \pm 5$ nm.

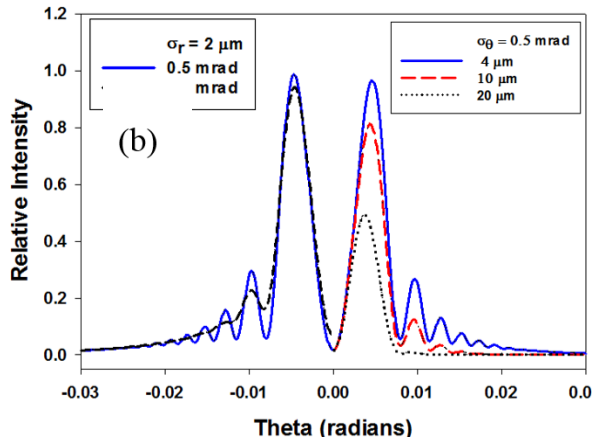


Figure 3: COTRI calculations for the effects of beam divergence ($\theta < 0$) for a fixed beam size of $2 \mu\text{m}$ and the effects of microbunched beam size on fringe intensity for a fixed beam divergence of 0.5 mrad ($\theta > 0$).

1.0-GeV COTRI Results

The next case considered was for 1-GeV electrons with a foil spacing, $L = 50.8$ mm, BPF of 633 ± 5 nm, and initial beam sizes of 10 and $30 \mu\text{m}$. Three polarization components are considered: the parallel component in the observation plane, I_{par} ; the perpendicular component to this plane, I_{perp} ; and the sum of these two components, I_{tot} , which is observed if no linear polarizer is used. With the low divergence of 0.1 mrad, the beam size changes in the drift of 50.8 mm are minimal in the I_{par} plot of Fig. 4a and are similar to Fig. 7a of reference [6] with a constant-beam-size model. However, with the larger divergence value of 0.7 mrad, the fringe visibility is greatly reduced in Fig. 4b, and the beam size changes from 10 to $36.9 \mu\text{m}$ in the drift. This also reduces the fringe peak intensities.

Interestingly, the interference terms result in the first lobes being at ± 2.8 mrad instead of at ± 0.5 mrad, the $1/\gamma$ value. This enables divergence sensitivity in the 0.1 to 0.5 mrad range in the central valley which normally would not be as accessible with the single-foil angular distribution pattern with the smaller $1/\gamma$ opening angle. This is true even for the $30\text{-}\mu\text{m}$ initial beam size with I_{tot} COTRI cases as shown in Fig. 5. We trade outer fringe visibility effects in the $10\text{-}\mu\text{m}$ case for the central minimum visibility effects with the larger $30\text{-}\mu\text{m}$ beam size.

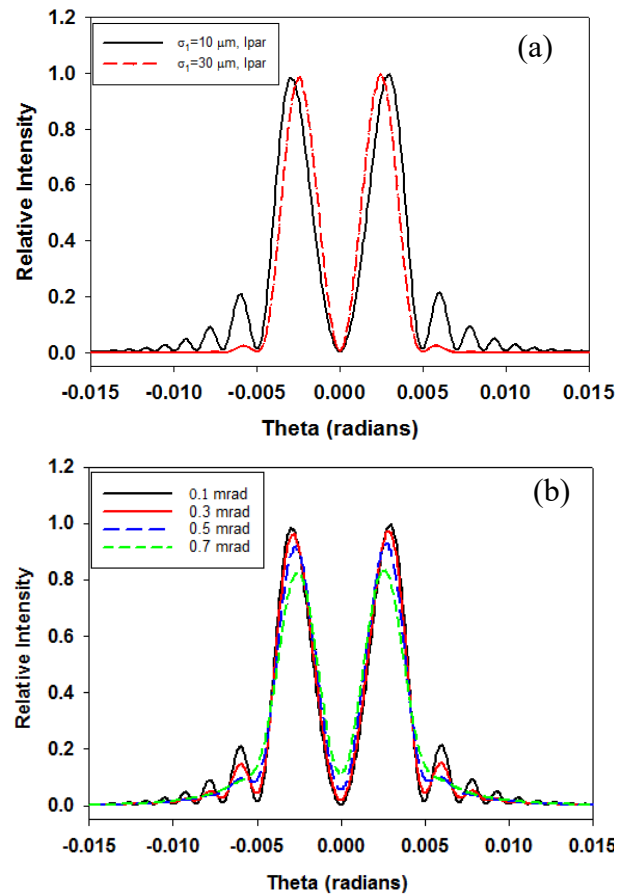


Figure 4: Plots of I_{par} COTRI patterns at 1.0 GeV for (a) two initial beam sizes σ_1 of 10 and $30 \mu\text{m}$ showing the coherence gain factor effects on the observed fringes for the parameters in text. Peaks at angles beyond ± 5 mrad have lower gain factors in the $\sigma_1 = 30\text{-}\mu\text{m}$ case. and (b) four divergence values for $\sigma_1 = 10 \mu\text{m}$ showing the effect on the central minimum and peaks 2,3 with reduced visibility at the $700\text{-}\mu\text{m}$ case with $\sigma_2 = 36.9 \mu\text{m}$ at foil 2.

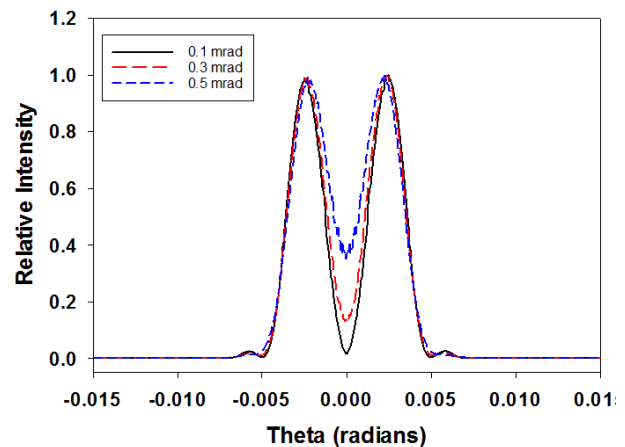


Figure 5: Plots of I_{tot} COTRI patterns at 1 GeV for an initial beam size σ_1 of $30 \mu\text{m}$ and divergences of 0.1 , 0.3 , and 0.5 mrad. The divergence sensitivity is in the central valley in these cases.

EXAMPLE EXPERIMENTAL RESULTS

Examples of the NF and FF images from the same LPA shot at 215 MeV from a previous experiment [6] are shown in Figs. 6 and 7, respectively. In Fig. 6a we see the vertically polarized COTR point spread function (PSF) lobes for two beamlets separated on the x axis (laser polarization axis) by about $6\ \mu\text{m}$. This is consistent with the earlier VORPAL simulations that exhibited a bimodal spatial distribution on the laser polarization axis, but not on the orthogonal axis [12]. A sample of the analysis technique which used the measured PSF lobe separation of $5.0\ \mu\text{m}$ in y to determine the vertical beam size of about $\sigma = 2.0\ \mu\text{m}$ is shown in Fig. 6b. In Fig. 7a, the FF COTRI pattern is shown whose fringe number and visibility are compared to Fig. 3 earlier model [8] results as well as the revised model [7] results to obtain a sub-mrad divergence of $0.4 \pm 0.2\ \text{mrad}$ and a beam size less than $4\ \mu\text{m}$. In addition, the analysis of the intensity of the FF image referenced to a calibrated laser source at 633 nm led to an estimated COTR gain $>10^5$ [7]. This is surprisingly similar to the SASE FEL COTR result at saturation [2], although the number of microbunched electrons in the LPA case is 30-50 times smaller, as is the beam distribution.

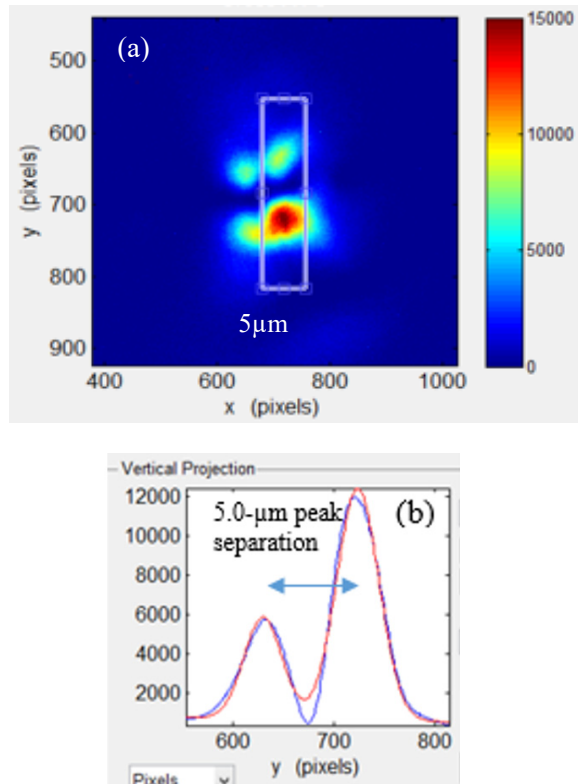


Figure 6: a) Vertically polarized NF image showing two pairs of coherent PSF lobes for two beamlets separated by about $6\ \mu\text{m}$. b) vertical profile of right hand beamlet with a $5\text{-}\mu\text{m}$ lobe separation which is mapped to $4.6\ \mu\text{m}$ (FWHM) or $2.0\ \mu\text{m}$ (σ).

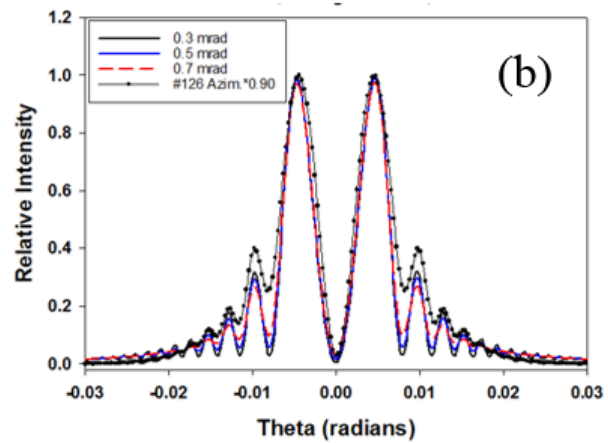
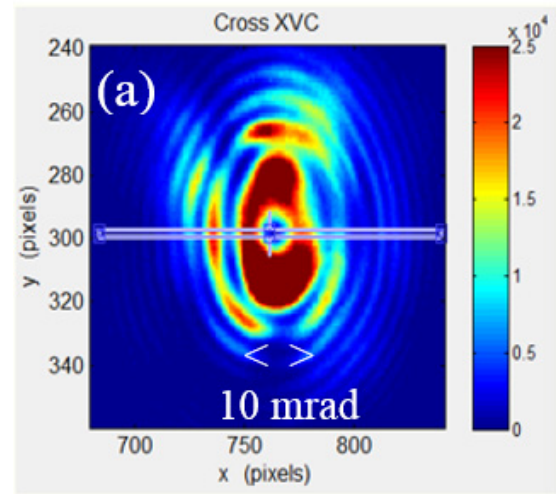


Figure 7: (a) Example of a FF COTRI image at $633 \pm 5\ \text{nm}$ from the same shot as Fig. 6. (b) Comparison of the azimuthally averaged over a quadrant data and the COTRI model for 0.3-, 0.5-, and 0.7-mrad divergence. The fringe peak positions are well matched, but the relative intensities of some outer fringes are higher in the data. The best match is 0.5 mrad.

SUMMARY

In summary, we have recalled a classic SASE FEL case where the electron microbunching was tracked as a function of z , and a COTRI model was applied [2]. We have compared that observed COTR gain seen at saturation to a recent LPA experiment that obtained single shot NF and FF images to determine beam size and divergence. We have noted the similar COTR gain $>10^5$ in the two experiments, although there is a marked difference in the transverse size of the microbunched portion. In the case of the LPA, this microbunching appears to be a fundamental aspect of the LPA process and merits further investigation. We also suggest that the LPA microbunching at the 1% level in a narrow band might be used to seed a visible light SASE FEL experiment by adding an undulator(s) downstream of the LPA.

ACKNOWLEDGEMENTS

The first author acknowledges the support of C. Drennan and M. Lindgren of the Accelerator Division at Fermilab. The University of Texas authors acknowledge support from DoE grant DE-SC0011617, and M.C.D. from the Alexander von Humboldt Foundation. The Helmholtz-Zentrum Dresden-Rossendorf author acknowledges support from the Helmholtz Association under program Matter and Technology, topic Accelerator R&D.

REFERENCES

- [1] K.-J. Kim, Z. Huang, and R. Lindberg, *Synchrotron Radiation and Free-Electron Lasers: Principles of Coherent X-ray Generation*. Cambridge, United Kingdom: Cambridge University Press, 2017. doi:10.1017/9781316677377
- [2] A. H. Lumpkin *et al.*, “Evidence for Microbunching “Sidebands” in a Saturated Free-Electron Laser Using Coherent Optical Transition Radiation”, *Phys. Rev. Lett.*, vol. 88, p. 234801, 2002. doi:10.1103/PhysRevLett.88.234801
- [3] Y. Glinec, J. Faure, A. Norlin, A. Pukhov, and V. Malka, “Observation of Fine Structures in Laser-Driven Electron Beams Using Coherent Transition Radiation”, *Phys. Rev. Lett.*, vol. 98, p. 194801, 2007. doi:10.1103/PhysRevLett.98.194801
- [4] C. Lin *et al.*, “Long-Range Persistence of Femtosecond Modulations on Laser-Plasma-Accelerated Electron Beams”, *Phys. Rev. Lett.*, vol. 108, p. 094801, 2012. doi:10.1103/PhysRevLett.108.094801
- [5] M. LaBerge *et al.*, “Observation of annular point spread function of optical transition radiation from low-emittance e-beams emerging from a laser-plasma accelerator”, presented at the 3rd European Advanced Accelerator Concepts Workshop. (EAAC’17), Elba, Italy, Sep. 2017, unpublished.
- [6] A. Lumpkin *et al.*, “Observations of Coherent Optical Transition Radiation Interference Fringes Generated by Laser Plasma Accelerator Electron Beamlets”, in *2018 IEEE Advanced Accelerator Concepts Workshop (AAC)*, Breckenridge, CO, United States, Aug. 2018, pp. 1-5. doi:10.1109/AAC.2018.8659381
- [7] A. H. Lumpkin *et al.*, “Coherent Optical Signatures of Electron Microbunching in Laser-Driven Plasma Accelerators”, *Phys. Rev. Lett.*, vol. 125, p. 014801, 2020. doi:10.1103/PhysRevLett.125.014801
- [8] D. W. Rule and A. H. Lumpkin, “Analysis of Coherent Optical Transition Radiation Interference Patterns Produced by SASE-Induced Microbunches”, in *Proc. 19th Particle Accelerator Conf. (PAC’01)*, Chicago, IL, USA, Jun. 2001, paper TPAH029, pp. 1288-1290. doi:10.1109/PAC.2001.986656
- [9] M. Migliorati *et al.*, “Intrinsic normalized emittance growth in laser-driven electron accelerators”, *Phys. Rev. ST Accel. Beams*, vol. 16, p. 011302, 2013. doi:10.1103/PhysRevSTAB.16.011302
- [10] U. Schramm *et al.*, “First results with the novel petawatt laser acceleration facility in Dresden”, *J. Phys.: Conf. Ser.*, vol. 874, p. 012028, 2017. doi:10.1088/1742-6596/874/1/012028
- [11] L. Wartski, S. Roland, J. Lasalle, M. Bolore, and G. Filippi, “Interference phenomenon in optical transition radiation and its application to particle beam diagnostics and multiple-scattering measurements”, *J. Appl. Phys.*, vol. 46, pp. 3644-3653, 1975. doi:10.1063/1.322092
- [12] A. H. Lumpkin, R. A. Crowell, Y. Li, and K. Nemeth, “A Compact Electron Spectrometer for an LWFA”, in *Proc. 29th Int. Free Electron Laser Conf. (FEL’07)*, Novosibirsk, Russia, Aug. 2007, paper WEAAU05, pp. 294-297.